Structural interactions of a voltage sensor toxin with lipid membranes

Mihaela Mihailescu[a,b,1], Dmitriy Krepkiy[c,1], Mirela Milescu[c,d], Klaus Gawrisch[e], Kenton J. Swartz[c,2], and Stephen White[f,2]

[a]Institute for Bioscience and Biotechnology Research, University of Maryland, Rockville, MD 20850; [b]National Institute of Standards and Technology Center for Neutron Research, National Institute of Standards and Technology, Gaithersburg, MD 20899; [c]Molecular Physiology and Biophysics Section, Porter Neuroscience Research Center, National Institute of Neurological Disorders and Stroke, National Institutes of Health, Bethesda, MD 20892; [d]Biology Division, University of Missouri, Columbia, MO 65211; [e]Laboratory of Membrane Biochemistry and Biophysics, National Institute on Alcohol Abuse and Alcoholism, National Institutes of Health, Bethesda, MD 20892; and [f]Department of Physiology and Biophysics, University of California, Irvine, CA 92697

Edited by Christopher Miller, Howard Hughes Medical Institute, Brandeis University, Waltham, MA, and approved October 22, 2014 (received for review August 11, 2014)

Protein toxins from tarantula venom alter the activity of diverse ion channel proteins, including voltage, stretch, and ligand-activated cation channels. Although tarantula toxins have been shown to partition into membranes, and the membrane is thought to play an important role in their activity, the structural interactions between these toxins and lipid membranes are poorly understood. Here, we use solid-state NMR and neutron diffraction to investigate the interactions between a voltage sensor toxin (VSTx1) and lipid membranes, with the goal of localizing the toxin in the membrane and determining its influence on membrane structure. Our results demonstrate that VSTx1 localizes to the headgroup region of lipid membranes and produces a thinning of the bilayer. The toxin orients such that many basic residues are in the aqueous phase, all three Trp residues adopt interfacial positions, and several hydrophobic residues are within the membrane interior. One remarkable feature of this preferred orientation is that the surface of the toxin that mediates binding to voltage sensors is ideally positioned within the lipid bilayer to favor complex formation between the toxin and the voltage sensor.

voltage sensor toxin | voltage-activated ion channel | toxin–membrane interaction | membrane structure | neutron diffraction

Protein toxins from venomous organisms have been invaluable tools for studying the ion channel proteins they target. For example, in the case of voltage-activated potassium (Kv) channels, pore-blocking scorpion toxins were used to identify the pore-forming region of the channel (1, 2), and gating modifier tarantula toxins that bind to S1–S4 voltage-sensing domains have helped to identify structural motifs that move at the protein–lipid interface (3–5). In many instances, these toxin–channel interactions are highly specific, allowing them to be used in target validation and drug development (6–8).

Tarantula toxins are a particularly interesting class of protein toxins that have been found to target all three families of voltage-activated cation channels (3, 9–12), stretch-activated cation channels (13–15), as well as ligand-gated ion channels as diverse as acid-sensing ion channels (ASIC) (16–21) and transient receptor potential (TRP) channels (22, 23). The tarantula toxins targeting these ion channels belong to the inhibitor cystine knot (ICK) family of venom toxins that are stabilized by three disulfide bonds at the core of the molecule (16, 17, 24–31). Although conventional tarantula toxins vary in length from 30 to 40 aa and contain one ICK motif, the recently discovered double-knot toxin (DkTx) that specifically targets TRPV1 channels contains two separable lobes, each containing its own ICK motif (22, 23).

One unifying feature of all tarantula toxins studied thus far is that they act on ion channels by modifying the gating properties of the channel. The best studied of these are the tarantula toxins targeting voltage-activated cation channels, where the toxins bind to the S3b–S4 voltage sensor paddle motif (5, 32–36), a helix-turn-helix motif within S1–S4 voltage-sensing domains that moves in response to changes in membrane voltage (37–41). Toxins binding to S3b–S4 motifs can influence voltage sensor activation, opening and closing of the pore, or the process of inactivation (4, 5, 36, 42–46). The tarantula toxin PcTx1 can promote opening of ASIC channels at neutral pH (16, 18), and DkTx opens TRPV1 in the absence of other stimuli (22, 23), suggesting that these toxin stabilize open states of their target channels.

For many of these tarantula toxins, the lipid membrane plays a key role in the mechanism of inhibition. Strong membrane partitioning has been demonstrated for a range of toxins targeting S1–S4 domains in voltage-activated channels (27, 44, 47–50), and for GsMTx4 (14, 50), a tarantula toxin that inhibits opening of stretch-activated cation channels in astrocytes, as well as the cloned stretch-activated Piezo1 channel (13, 15). In experiments on stretch-activated channels, both the D- and L-enantiomers of GsMTx4 are active (14, 50), implying that the toxin may not bind directly to the channel. In addition, both forms of the toxin alter the conductance and lifetimes of gramicidin channels (14), suggesting that the toxin inhibits stretch-activated channels by perturbing the interface between the membrane and the channel. In the case of Kv channels, the S1–S4 domains are embedded in the lipid bilayer and interact intimately with lipids (48, 51, 52) and modification in the lipid composition can dramatically alter gating of the channel (48, 53–56). In one study on the gating of the Kv2.1/Kv1.2 paddle chimera (53), the tarantula toxin VSTx1 was proposed to inhibit Kv channels by modifying the forces acting between the channel and the membrane. Although these

Significance

Tarantula venom contains protein toxins that interact with diverse families of ion channels and alter their activity. A number of tarantula toxins are known to interact with membranes and are thought to bind to ion channel proteins within the lipid bilayer. In the present study, we find that tarantula toxins influence the structure and dynamics of the lipid bilayer, and that the toxin orients itself within membranes to facilitate formation of the toxin–channel complexes. Our results have implications for the mechanisms of toxin action on ion channels, and more generally for protein–protein interactions within membranes.

Author contributions: M. Mihailescu, D.K., M. Milescu, K.G., K.J.S., and S.W. designed research; M. Mihailescu, D.K., M. Milescu, and K.G. performed research; M. Mihailescu, D.K., M. Milescu, and K.G. analyzed data; and M. Mihailescu, D.K., M. Milescu, K.G., K.J.S., and S.W. wrote the paper.

The authors declare no conflict of interest.

This article is a PNAS Direct Submission.

Freely available online through the PNAS open access option.

[1]M. Mihailescu and D.K. contributed equally to this work.

[2]To whom correspondence may be addressed. Email: swartzk@ninds.nih.gov or Stephen.white@uci.edu.

This article contains supporting information online at www.pnas.org/lookup/suppl/doi:10.1073/pnas.1415324111/-/DCSupplemental.

studies implicate a key role for the membrane in the activity of Kv and stretch-activated channels, and for the action of tarantula toxins, the influence of the toxin on membrane structure and dynamics have not been directly examined. The goal of the present study was to localize a tarantula toxin in membranes using structural approaches and to investigate the influence of the toxin on the structure of the lipid bilayer.

Results

To obtain large quantities of the peptide essential for structural studies, we folded synthetic VSTx1 in vitro from its linear form using controlled air oxidation (27). As previously described, the folded toxin displayed a shorter retention time when analyzed using reversed-phase HPLC chromatography (Fig. 1*A*) and was active against a chimeric Kv channel in which the paddle motif of KvAP was transplanted into Kv2.1 channel (5) (Fig. 1*B*). We also confirmed that the folded toxin favorably partitions into membranes using intrinsic Trp fluorescence of the toxin. VSTx1 contains three Trp residues (at position 7, 25, and 27), and when excited at 280 nm, the emission spectrum of the toxin exhibits a blue shift when small unilamellar vesicles (SUVs) containing a 1:1 mixture of 1-palmitoyl-2-oleoyl-*sn*-glycero-3-phosphocholine (POPC):1-palmitoyl-2-oleoyl-*sn*-glycero-3-[phospho-*rac*-(1-glycerol)] (POPG) are added to the solution (Fig. 1*C*), indicating that the toxin interacts with membranes. Titration of the lipid concentration in these experiments yields a mole fraction partition coefficient of $1.46 \pm 0.14 \times 10^5$ (Fig. 1*D*), consistent with previous results (27). To provide an initial estimate of the depth of VSTx1 partitioning, we measured quenching of Trp fluorescence by bromine atoms attached to different positions of the acyl chain of POPC (Fig. 1 *E*–*G*). Quenching was most pronounced when examining lipids with bromine attached near the middle of the acyl chain (9,10-diBr), and analysis of the quenching profile yielded a value of 9 Å from the center of the bilayer (Fig. 1*F*), consistent with what has been reported for related tarantula toxins hanatoxin and SGTx1 (3, 44, 57). These data do not provide a reliable measure of the depth of tarantula toxin partitioning into membranes (58) because there is substantial thermal disorder of both the quenching lipids and of the fluorophore, deformations of the membrane around the toxin, as well as the presence of three Trp residues in VSTx1. However, these results support the notion that the toxin interacts intimately with the membrane and adopts an interfacial position. We also obtained CD spectra of VSTx1 in the presence and absence of SUVs and could not detect any change in the secondary structure upon partitioning into membranes (Fig. S1).

Influence of VSTx1 on Structural Dynamics of Membranes. To begin our investigation into the influence of tarantula toxins on membrane structure, we undertook solid-state NMR experiments that allow us to detect possible effects of the toxin on the dynamics of lipid acyl chains. For this purpose, we prepared oriented multilayer samples of membranes using a 1:1 mixture of POPC and POPG with a perdeuterated palmitoyl chain (D31; Fig. 1*G*) in either POPC (D31-POPC) or POPG (D31-POPG), both in the presence and absence of VSTx1 (*Experimental Procedures*). We then obtained ^{2}H NMR spectra on these samples as described (59, 60). Inspection of these spectra (Fig. 2*A*) reveals that VSTx1 incorporation into bilayers reduces ^{2}H NMR quadrupolar splittings of the perdeuterated palmitoyl chains, indicating that the toxin decrease the order parameters of the lipid acyl chains. We calculated order parameters [$S(n)$] for C–D bonds for all positions along the acyl chain, and observed profiles that are typical of lipid bilayers, with a progressive reduction of the order parameters between the middle of the hydrocarbon chain and the terminal methyl group (Fig. 2*B*). VSTx1 decreased the order parameters for all hydrocarbon chain segments, with the largest perturbations being observed for carbon atoms between 2 and 10 (Fig. 2*B*). The observed reduction in lipid order upon VSTx1 partitioning results from an increase in the lateral area of the lipid bilayer and a decrease in the bilayer thickness. We also calculated changes in the hydrophobic thickness (61) and found that the thickness of the bilayer decreased in the presence of toxin, with a maximum reduction of ~2.5 Å (Fig. 2*D*). Because previous studies with VSTx1 and a related tarantula toxin have shown that negatively charged lipids enhance the strength of toxin–membrane interactions (27, 47), we also compared the effects of VSTx1 on fully hydrated proteoliposome samples in which the palmitoyl chain of POPC was perdeuterated in 1:1 mixtures of POPC:POPG with those produced with perdeuterated POPG. VSTx1 decreased the order parameters in these proteoliposome experiments (Fig. S2), similar to what we observed with oriented multilayers (Fig. 2), and the effects of the toxin on order parameters of the two lipid preparations were similar (Fig. S2, compare *A* and *B* with *C* and *D*), indicating that we cannot detect any preferential interactions of these lipids with VSTx1. Overall, the VSTx1-induced changes in lipid order parameter profiles demonstrates that the toxin perturbs the structure and dynamics of lipid membranes, with a pattern that supports an interfacial location of the toxin in the lipid bilayer.

Structure and Hydration of Membranes Containing VSTx1. To explore the changes in membrane structure more directly, we undertook neutron diffraction experiments using hydrogen-deuterium contrast analysis with deuterium-labeled lipids, water, or VSTx1, taking advantage of the contrasting negative scattering-length density (SLD) of hydrogen and the positive SLD of deuterium (62) (Tables S1–S3). To determine the profile structure of bilayers in the presence and absence of VSTx1, oriented POPC:POPG multilayers were hydrated (86% relative humidity) and mounted in a cold neutron beam (63), resulting in strong lamellar diffraction patterns with Bragg spacing (d) (Fig. S3). One-dimensional, absolute-scale, SLD profiles along the normal to the lipid bilayer plane were then constructed (Fig. 3*A*), which in the case of neat hydrogenated lipid bilayers (black solid line) show positive densities for the headgroup region, a trough for the hydrocarbon tails, and negative densities near the terminal methyl groups. In comparison, the lipid bilayer profile in the presence of VSTx1 (green solid line) shows an increase in density near the headgroup region of the bilayer, consistent with an interfacial localization of the toxin (Fig. 3*A*). Importantly, the toxin produces a detectable thinning of the bilayer, with a decrease in d of about 2 Å at protein-to-lipid ratios (molar) of 1:30 (Fig. 3*B*). To directly investigate the influence of VSTx1 on the hydrocarbon core of the bilayer, we constructed SLD profiles using POPG in the absence (black dashed line) and presence (green dashed line) of VSTx1. Deuterium difference profiles obtained by subtracting profiles for hydrogenated lipid samples from those for deuterated lipid samples yield, specifically, the profiles for the hydrocarbon chains of the membrane (black and green dashed-dotted lines) (Fig. 3*A*). Comparison of these profiles demonstrates that the toxin thins the hydrocarbon core of the membrane, consistent with the solid-state NMR results. If we define the hydrocarbon thickness as the full width at half-maximum of the chain profiles (Fig. 3*A*), and assume that the volume of the chain segments are close to the values corresponding to liquid hydrocarbons ($V_{CH2} = 27$ Å^3, $V_{CH3} = 54$ Å^3, and $V_{CH} = 20.5$ Å^3 at 25 °C) (64), the area per lipid, along the bilayer surface, increases from ~59 Å^3 for the neat bilayer to ~63 Å^3 in the presence of 1 mol% VSTx1. This shows that the area of the lipid membrane expands in the presence of the toxin, under the condition of constant volume of the hydrocarbon.

We also constructed water profiles by comparing bilayer profiles obtained in the presence of H_2O and ^2H_2O, which show that 1.75% VSTx1 broadens the water distribution and increases the number of waters in the bilayer (Fig. 3*C*). The water distribution

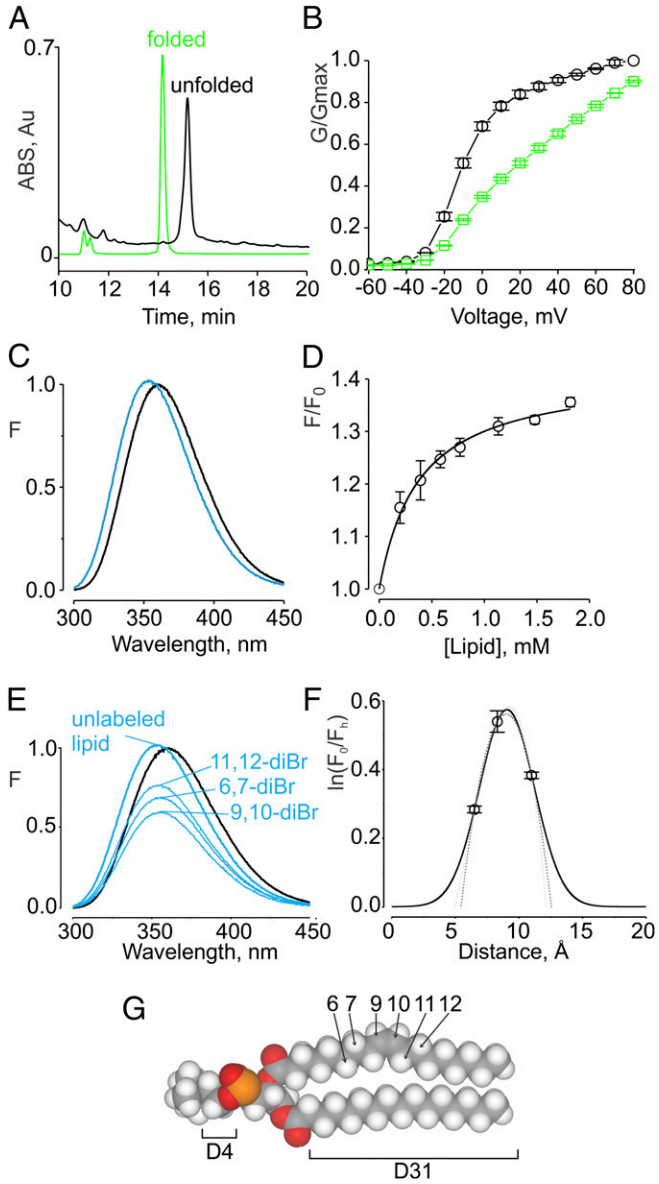

Fig. 1. Production and characterization of synthetic VSTx1. (*A*) HPLC chromatogram of synthetic patch deuterated VSTx1 before and after folding. Absorbance at 215 nm is plotted against elution time. The elution gradient was from 20% (vol/vol) CH_3CN in water with 0.1% TFA to 100% CH_3CN with 0.1% TFA over 50 min. Retention time of synthetic folded peptide is identical to the native peptide purified from *Grammostola spatulata* venom (27). (*B*) Inhibition of Kv2.1/KvAP chimera (5) by synthetic patch deuterated VSTx1. VSTx1 peptide was dissolved in trifluoroethanol:hexafluoroisopropanol (1:2) mixture, dried under the N_2 flow, and dissolved in buffer for Kv channel recordings (50 mM KCl, 50 mM NaCl, 1 mM $MgCl_2$, 0.3 mM $CaCl_2$, 20 mM Hepes, pH 7.4). The chimeric Kv2.1/KvAP channel was expressed in oocytes and membrane voltage controlled using a two-electrode voltage clamp, as previously described (5). Macroscopic potassium currents were elicited by membrane depolarization from a holding voltage of −80 mV, and conductance (G/G_{max}) was obtained from tail current measurements at −60 mV following each test depolarization either in control solution (black) or the presence of 4 μM VSTx1 (green). (*C*) Fluorescence emission spectra for VSTx1 in the absence (black) and presence of lipid vesicles (1.3 mM) composed of a 1:1 mix of POPG and POPC (blue). Excitation wavelength was 280 nm. (*D*) Fluorescence intensity at 320 nm plotted as a function of available lipid concentration (60% of total lipids). Smooth curves correspond to a partition function (*Experimental Procedures*) with $K_x = (1.46 \pm 0.14) \times 10^5$ and $F/F_0^{max} = 1.41 \pm 0.013$. Data points are the mean ± SEM ($n = 3$). (*E*) Depth-dependent quenching of tryptophan fluorescence by brominated phosphatidylcholines. Fluorescence emission spectra for VSTx1 in the absence and presence of lipid vesicles containing unlabeled or brominated (diBr) lipids (1.3 mM). (*F*) Analysis of the depth-dependent quenching profiles for VSTx1. Fractional quenching (F_0/F_h) by brominated lipids plotted as a function of the average distance of bromine atoms from the center of the bilayer. The solid lines correspond to DA analysis, where $h_m = 9$ Å, $S = 0.46$, $\sigma = 1.18$ Å; and dashed lines correspond to PM analysis, where $h_m = 9$ Å, $f = 17$, $R_c = 3.5$ Å. Data points are the mean ± SEM ($n = 3$). (*G*) Positions labeled on POPC with either deuterium (^2H) or bromine (Br). D4 contains 4 ^2H on the choline headgroup, and D31 contains 31 ^2H on the palmitoyl chain. Two Br atoms were incorporated on carbons of the oleoyl chain at positions 6 and 7 (6,7-diBr), 9 and 10 (9,10-diBr), or 11 and 12 (11,12-diBr).

broadens in the presence of VSTx1 from 13.6 ± 0.1 to 14.3 ± 0.2 Å full width at half-maximum. After scaling to D4 lipids (*Experimental Procedures*; Fig. 1*G*), the number of water molecules per composition unit cell (0.0175 VSTx1 molecules and 0.9925 lipid molecules) was determined to be 9.3 ± 0.4. We measured a value of 8.1 ± 0.7 waters per unit cell previously for the neat POPC:POPG lipid mixture at the same hydration (62). This result indicates that hydration of the bilayer is increased by ∼65 H_2O molecules per toxin. This broadening of the water distribution and the increase in the number of waters per unit cell, together indicate that a shell of water molecules is associated with the toxin in the lipid bilayer.

Position of VSTx1 in Membranes. The results presented thus far suggest that VSTx1 adopts an interfacial localization when it partitions into membranes. To localize the toxin within the structure of lipid bilayers directly, we undertook neutron diffraction experiments to compare membranes containing deuterated and hydrogenated VSTx1. The deuterated toxin was produced by synthesizing the toxin with deuterated side chains at five positions forming a hydrophobic patch (8 ^2H in F5, 5 ^2H in W7, 3 ^2H in M6, 8 ^2H in V29, and 10 ^2H in L30; 34 deuterium atoms total). The deuterated toxin retained 96% of the expected deuterium atoms after folding, as determined by mass spectrometry analysis. Samples with hydrogenated and deuterated VSTx1 were characterized by the same repeat spacing (Fig. S3*B*; 51.2 ± 0.1 Å), indicating that the samples were identical except for the presence of deuterium. The distribution of the deuterated patch of the toxin, in projection on the normal to the bilayer plane (Fig. 4), had a center-of-mass at 18.0 ± 0.2 Å from the bilayer center with a full width at half-maximum of ∼8 Å, and displayed a non-Gaussian shape. In comparison, the distribution of deuterium atoms for membranes containing POPC deuterated in the headgroup methylenes (D4 lipid; Fig. 1*G*) was well described by a Gaussian distribution with a mean position at 20.16 ± 0.2 Å and a full width at half-maximum of 6.9 ± 0.5 Å (Fig. 4). The maxima in the SLD profiles of the bilayer due to the contribution from carbonyl and phosphodiester groups of the lipid are located at 17 Å from the bilayer center, which by comparison with the toxin profiles would also support a relatively superficial position of the toxin in POPC:POPG membranes.

Orientation of VSTx1 in Membranes. To constrain the orientation of VSTx1 in membranes, we used the solution structure of the toxin (27), replaced 34 hydrogen atoms in the hydrophobic patch with deuterium atoms, and then computed the projection of the deuterium atoms distributions on the normal to the bilayer (z axis). We then performed rigid body rotations and translation of the toxin until the deuterium distribution most closely approximated the experimentally determined profile (Fig. 5 and Fig. S4). In the preferred orientation of VSTx1, the toxin is located superficially at the lipid–water interface and orients such that its hydrophobic C terminus (V29, L30, A31, P33, and F34) positions deeper into the membrane than residues on the opposite side. The three Trp residues (W7, W25, W27) form a ridge that aligns along the water–hydrocarbon interface (Fig. S5). The

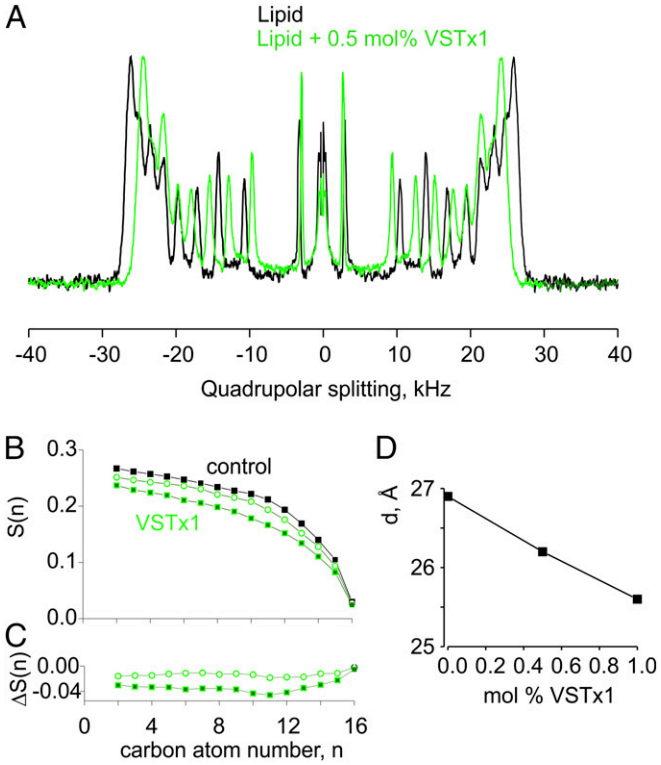

Fig. 2. ^{2}H solid-state NMR determination of order parameters of C–D bonds for palmitoyl chain of POPC in the absence or presence of the peptide VSTx1. (*A*) ^{2}H NMR spectra of oriented bilayers of [16:0(D31)-18:1n9-POPC]:(16:0-18:1n9-POPG) (1:1) in the presence or absence of VSTx1 at 86% relative humidity and 303.1 K. ^{2}H NMR spectra were acquired on oriented bilayers with a quadrupolar echo pulse sequence on a Bruker AV800 MHz spectrometer. The bilayer normal is oriented parallel to the magnetic field. (*B*) ^{2}H NMR order parameters, *S*(*n*), of the palmitoyl chain of POPC in the absence or presence of the peptide VSTx1. (*C*) VSTx1-induced difference on the palmitoyl hydrocarbon chain order of D31-POPC in a D31-POPC:POPG (1:1) mixture. The 0.5 mol% VSTx1 (1 (open green circles) and 1 mol% VSTx1 (filled green symbols). (*D*) VSTx1-induced changes of hydrophobic thickness of the bilayer, *d*, calculated from the averaged order parameter of the D31-palmitoyl hydrocarbon chain of POPC.

deuterated patch is situated right below this ridge, with its center of mass positioned at 18 Å from the bilayer center. Many of the basic residues (R24, K26, K4) project outside the hydrophobic phase of the membrane, and into the water phase. However, K17 and D18 project toward the bilayer interior, which would suggest that they must form a salt bridge. This proposed orientation of VSTx1 is compatible with previous results with the related tarantula toxin SGTx1, in which transferred cross-saturation NMR experiments were used to measure magnetization transfer between lipids and the toxin (57).

Discussion

The goal of the present study was to determine the influence of tarantula toxins on the structure and dynamics of lipid bilayers and to establish the disposition of the toxin in the membrane. The results of our solid-state NMR experiments demonstrate that VSTx1 decreases the order parameters of POPC and POPG (Fig. 2*A* and Fig. S2), leading to a thinning of the lipid membrane (Fig. 2 *A* and *B*). The results of neutron diffraction experiments also demonstrate that the toxin produces a thinning of the membrane (Fig. 3 *A* and *B*), in quantitative agreement with the solid-state NMR results and with earlier molecular-dynamics simulations (65). Partitioning of the VSTx1 into the membrane also broadens the water distribution determined using neutron diffraction (Fig. 3*C*), indicating that a shell of waters enters the bilayer along with the toxin. Although previous studies have concluded that tarantula toxins adopt relatively superficial positions when they partition into lipid membranes (44, 47, 57), these studies did not directly investigate the position and orientation of the toxins within the bilayer. Taking advantage of the negative and positive SLDs of hydrogen and deuterium, respectively, we labeled five residues on VSTx1 with deuterium and localized those atoms in membranes and compared those to the position of specifically deuterated lipid headgroups. The results of these experiments unambiguously demonstrate that the toxin adopts an interfacial localization in the membrane (Fig. 4), coinciding with the polar headgroups of lipids and overlapping the distributions of both water and D4-labeled lipids.

The voltage-sensing domains within Kv channels and other types of voltage-activated cation channels are common targets for tarantula toxins like VSTx1 (3, 40). Extensive mutagenesis within S1–S4 domains has identified the S3b–S4 paddle motif as a particularly important motif for the actions of tarantula toxins (5, 32, 34, 36, 44, 46, 48, 66), and it is this motif that moves in response to changes in voltage to open voltage-activated channels (40, 41). In keeping with the region of the channel they target, tarantula toxins can either retard or facilitate opening of Kv channels (5, 26, 33, 36, 42, 46, 48). Tarantula toxins are thought to interact with S1–S4 domains of Kv channels within

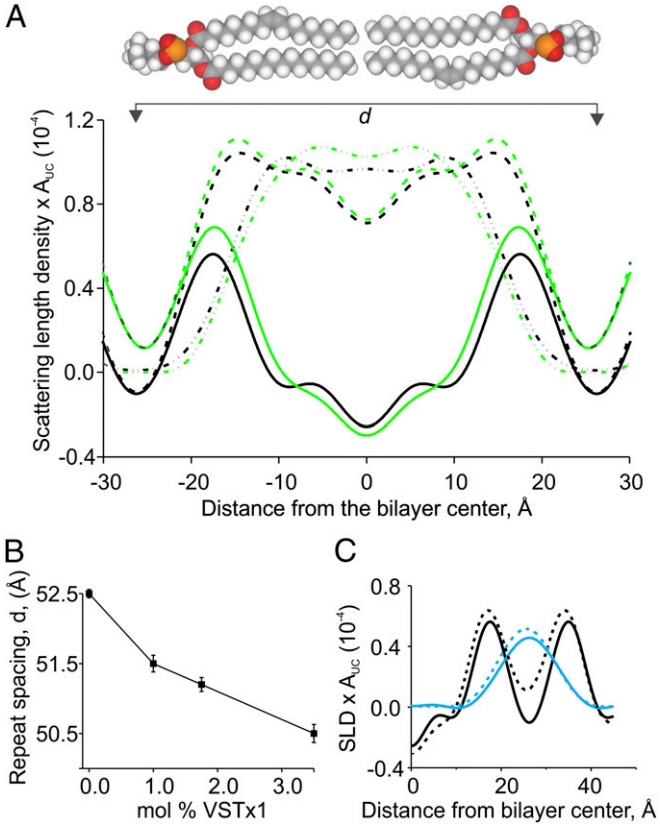

Fig. 3. Scattering-length density (SLD) profiles of bilayers with and without VSTx1. (*A*) SLD profile of an unlabeled (1:1 POPC:POPG) lipid bilayer (solid lines), a chain-deuterated (1:1 POPC:D31-POPG) bilayer (dashed lines), and their difference (dashed-dot-dashed lines). Profiles for samples without toxin are shown in black and with 1 mol% VSTx1 in green (Table S1). (*B*) Toxin-induced decrease in the repeat spacing of the lipid bilayer. (*C*) Effects of VSTx1 on the water distribution in the bilayer. SLD profiles (black) and water distribution (blue) of the POPC:POPG (1:1) bilayers in the absence (solid lines) or presence of 1.75 mol% VSTx1 (dashed lines).

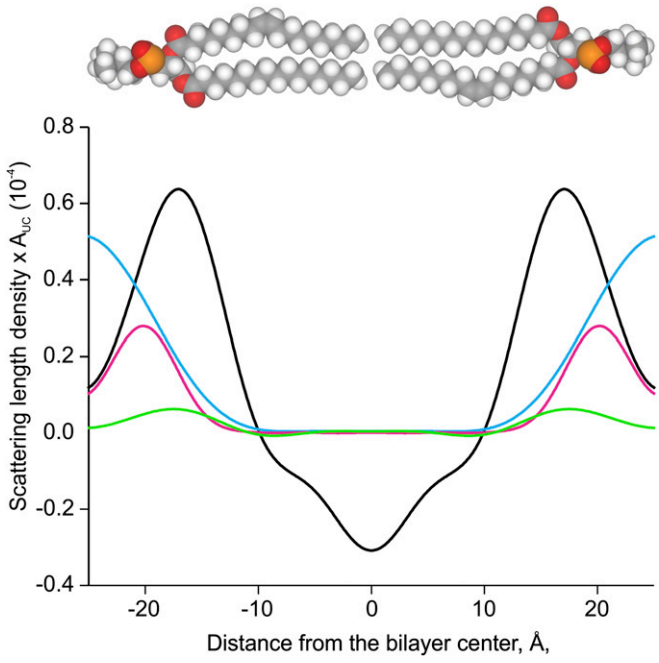

Fig. 4. Distribution of labeled VSTx1 in lipid bilayers. The SLD profile of the deuterated patch of VSTx1 (green) was determined by deuterium difference analysis. For comparison, the overall profiles of the bilayer (black) and water determined by $^{1}H_2O/^{2}H_2O$ exchange (blue) are shown in the presence of unlabeled VSTx, as well as for the $–(CH_2–CH_2)–$ of deuterated lipid headgroups (D4 lipid; purple). Calibrated structure factors corresponding to these profiles are shown in Table S2.

the membrane, as many of these toxins partition into membranes (27, 44, 47–49, 57), interact with the channel with high affinity when embedded in membranes, but only weakly when solubilized with detergents (49). Toxin mutations have also been identified that exhibit correlated effects on the strength of membrane partitioning and apparent affinity for binding to Kv channels (47), implicating membrane partitioning as an important component of the toxin mechanism. Experiments examining the interplay between Kv channel mutations and modification of sphingomyelin also support the idea that tarantula toxins bind to voltage sensors within the membrane (48).

Although the prevailing evidence suggests that tarantula toxins influence the gating of voltage-activated channels by binding within the membrane, how they influence voltage sensor movement is at present poorly understood. One possibility is that the protein–protein interface between toxin and S1–S4 domain rearranges as the domain moves, and that the toxin simply binds tighter to the conformation it stabilizes. Another possibility is that the toxin–membrane interaction rearranges as the S1–S4 domain changes conformation, and the toxin stabilizes the state of the voltage sensor in which it has the most favorable membrane interactions. A third possible mechanism was advanced by MacKinnon and colleagues when they discovered that the actions of VSTx1 on the Kv1.2/2.1 paddle chimera were dependent on the mechanical state of the lipid membrane (53). They compared the gating properties of the channel after reconstitution into black lipid membranes (BLMs) with that observed after expression in oocytes using either two-electrode voltage-clamp (TEVC) or patch-clamp recording techniques. The gating properties of the Kv channel varied considerably from BLMs to oocytes using TEVC, and patch recordings display a range of intermediate phenotypes. The key observation was that VSTx1 had little effect on the channel when studied in oocytes with TEVC, but the toxin transformed the gating properties of the channel observed in BLMs to resemble those studied with TEVC, as if the toxin modifies gating by altering the forces acting between the channel and the membrane. The effects we observed on VSTx1 diminishing the order parameters of acyl chains, thinning of the lipid bilayer, and facilitating the entry of water into the membrane, provide direct experimental support for the idea that tarantula toxins may influence Kv channel gating by perturbing the membrane–channel interface. Our results also provide support for the related model for inhibition of stretch-activated channels by GsMTx-4 (14).

We also investigated a range of different orientations of VSTx1, computed their predicted deuterium distributions, and compared those with our experimental distributions for the deuterium-labeled toxin (Fig. 5*A*). The computed orientation of the toxin that best reproduces our experimental deuterium distributions has several interesting features (Fig. S5). First, the preferred orientation positions many basic residues on a back side of the toxin such that their side chains project into the aqueous phase outside the membrane. Second, this orientation positions all three Trp residues within the interfacial region of the bilayer, consistent with the canonical view that Trp residues favor this region of the lipid membrane (67). Third, in the preferred orientation, both K17 and D18 insert into the hydrophobic core of the membrane along with hydrophobic residues in the C terminus of the toxin (e.g., V29, L30, A31, P33, and F34). Although the deep penetration of K17 and D18 was unexpected, these residues are within hydrogen-bonding distance in the NMR solution structure of VSTx1 (27) and thus could be stabilized within the hydrophobic core of the membrane by a salt bridge. Finally, the preferred orientation is interesting when examined in the context of earlier mutagenesis studies with the related tarantula toxin SGTx1. The first of these studies identified an active surface of the toxin where mutations weaken the apparent affinity of the toxin for the Kv2.1 channel (68), and the second investigated to what extent these mutations alter partitioning into lipid membranes (47). Five residues in SGTx1 (R3, L5, F6, R22, and W30) stand out as having disproportionally large effects on apparent affinity compared with membrane partitioning, and these cluster together on a surface of the toxin that is likely involved in protein–protein interactions with the voltage-sensing domains in the Kv channel. When these residues are mapped onto the structure of SGTx and the toxin oriented by superimposition on the preferred orientation of VSTx1 (Fig. 5 *B* and *C*), the residues predicted to be involved in protein–protein interactions are positioned laterally on one side of the toxin. This implies that the orientation of tarantula toxins in membranes has evolved to facilitate docking on voltage sensors as the toxins laterally diffuse through lipid bilayers. In the future, it will be interesting to explore the relative contributions of protein–protein and protein–lipid interactions in the mechanisms by which tarantula toxins influence the gating of ion channels proteins, and to further explore the structural basis of this fascinating ternary complex between toxin, channel, and membrane lipids.

Experimental Procedures

VSTx1 Folding, Purification, and Characterization. The linear form of synthetic VSTx1 was purchased as a TFA salt from Anaspec. The peptide was folded using a controlled air oxidation method and purified as previously described using ion exchange CM52 resin and reversed-phase high-performance liquid chromatography (HPLC) using a 5-μm, 90-Å, C-18 column (Beckman) (27). The concentration of the peptide in aqueous solution was determined using an extinction coefficient ε^{280} = 17,430 $M^{-1}{\cdot}cm^{-1}$. The concentration of peptide in mixtures of trifluoroethanol and hexafluoroisopropanol was determined using HPLC reverse-phase chromatography, integrating the peak corresponding to VSTx1. VSTx1 deuterated on the side chains of five residues (8 ^{2}H in F5, 5 ^{2}H in W7, 3 ^{2}H in M6, 8 ^{2}H in V29, and 10 ^{2}H in L30; 34 deuterium atoms total) was purchased from Anaspec in linear form as TFA salt and folded as with the hydrogenated toxin. Folded peptides were analyzed by TOF-MS electrospray and MALDI-MS at the National Institute of Neurologi-

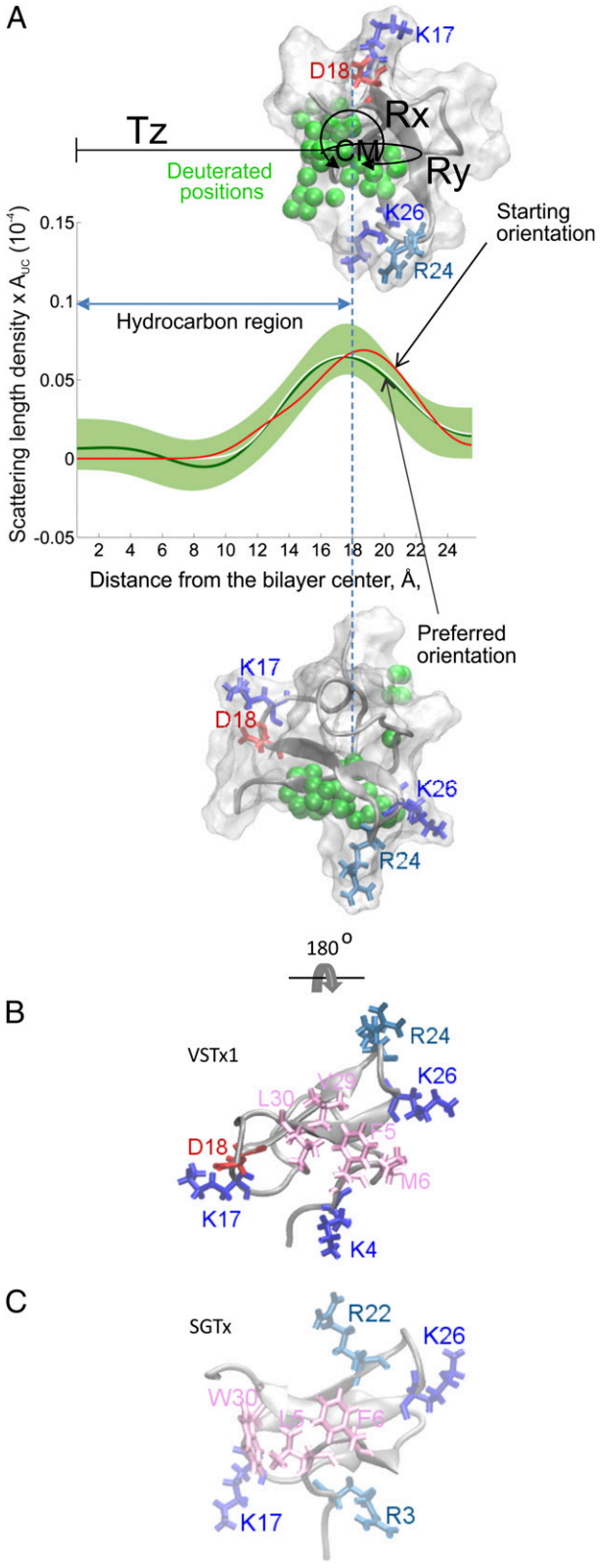

Fig. 5. Modeling of the preferred orientation of the VSTx1 in lipid bilayers. (*A*) Deuterium atoms were replaced for hydrogens at specific positions on the side chains of the "hydrophobic patch" of VSTx1 (8 ^{2}H in F5, 5 ^{2}H in F7, 3 ^{2}H in M6, 8 ^{2}H in V29, and 10 ^{2}H in L30) using the solution structure (accession code 1S6X). Each deuterium atom was described by Gaussian distributions centered at position (z_D) with a width governed by the Debye–Waller factor (*B*) (*Experimental Procedures*). Rigid body rotations (*Rx*, *Ry*) and translation (*Tz*) were applied until the projection of the deuterium atom distribution on the normal to the bilayer (red line) met the experimental SLD profile (dark green line). The preferred toxin orientation was determined with parameters of the best model fit (white). The uncertainty band (thick light green) was determined by a Monte Carlo sampling method (*Experimental Procedures*) and includes uncertainties in the measured structure factors due to counting statistics and uncertainties in the amplitude scaling factors due to sample composition. (*B*) VSTx1 in the preferred orientation, showing a cluster of hydrophobic amino acids pointing toward the hydrocarbon core and basic residues pointing toward the aqueous phase. (*C*) SGTx oriented by superimposition on the VSTx1 structure in the preferred orientation. The surface shown, containing R3, L5, F6, R22, and W30, has been implicated in binding to voltage-sensing domains.

cal Disorders and Stroke (NINDS) peptide sequencing facility to determine retention of deuterium atoms. CD spectra of the toxin were recorded in 20 mM Tris·HCl, 100 mM KCl buffer, pH 7.4, using a JASCO J-815 spectropolarimeter, from 180 to 250 nm with 1-nm step resolution and 4-s integration time. Functional activity of the synthetic folded VSTx1 toxin (Fig. 1*B*) was tested using a chimeric Kv channel containing the paddle motif of KvAP transplanted into the Kv2.1 channel, as previously described (5).

Fluorescence Spectroscopy. Large unilamellar vesicles (LUVs) were formed by extrusion of lipid mixtures (1:1 molar ratios) of POPG and either POPC, 6,7-diBr, 9,10-diBr, or 11,12-diBr [1-palmitoyl-2-stearoyl(dibromo)-*sn*-glycero-3-phosphocholine] (Avanti Polar Lipids). LUVs were added to an aqueous solution of toxin (2 μM final concentration in 10 mM Hepes, 1 mM EDTA, pH 7.0), maintained at 25 °C with continuous stirring. Fluorescence spectra (averaging of three spectra) were recorded between 300 and 400 nm (5-nm bandpass, 0° polarizer) using an excitation wavelength of 280 nm (5-nm bandpass, 90° polarizer) (SPEX FluoroMax 3 spectrofluorometer), corrected for vesicle scattering (69), and normalized to the zero lipid fluorescence intensity (F_0) at 320 nm. The mole-fraction partitioning coefficient (K_x) was calculated based on the best fits of the following equation to the data: $F/F_0(\mathrm{L}) = 1 + (F/F_0^{\max} - 1)\ K_x\ [\mathrm{L}]/([\mathrm{W}] + K_x\ [\mathrm{L}])$, where F/F_0(L) is the change in fluorescence intensity for a given concentration of lipid, $F/F_0^{\max}$ is the maximum fluorescence increase at high lipid concentrations, [L] is the average available lipid concentration (60% of total lipid concentration), and [W] is the molar concentration of water (55.3 M). The quenching of tryptophan fluorescence was examined at three lipid concentrations (0.3, 0.6, 1.3 mM) and quenching profiles were analyzed using both distribution analysis and the parallax method (70, 71). The average insertion depth of the tryptophan residue (h_m) was calculated based on best fits of the following equations to the data: DA, $\ln(F_0/F_h) = S/(\sigma\sqrt{2\pi})\exp(-(h - h_m)^2/2\sigma^2)$; PM, $\ln(F_0/F_h) = \pi C f[R_c^2 - (h - h_m)^2]$ when $h - h_m < R_c$, and $\ln(F_0/F_h) = 0$ when $h - h_m \geq R_c$. F and F_0 are the fluorescence intensities in the absence and presence of the diBr quenchers, h is the depth of the quencher based on X-ray diffraction measurements (72), C is the quencher concentration, σ is dispersion, S is area, R_c is radius of quenching, and f is fraction of the quencher in the tryptophan vicinity.

Solid-State ^{2}H NMR Spectroscopy. ^{2}H solid-state NMR spectroscopy was used to measure the order parameters, $S(n)$, for methylene and terminal methyl segments of the palmitoyl chain of 1-palmitoyl$_{d31}$-2-oleoyl-*sn*-glycero-3-phosphocholine (D31-POPC), or 1-palmitoyl$_{d31}$-2-oleoyl-*sn*-glycero-3-phospho-(1′-*rac*-glycerol) (D31-POPG) in the POPC:POPG (1:1) mixture in the absence or presence of the peptide VSTx1 (VSTx:lipid ratio of 1 mol%). The POPC:POPG prepared with either D31-POPC or D31-POPG were dried from chloroform solution under N_2 and in vacuum and resuspended in 20 mM Tris·Cl, pH 7.4. The lipid mixture was passed through a polycarbonate filter (100 nm) using an Avestin extruder. VSTx1 was added to liposome emulsion in different ratios and incubated at room temperature for 2 h. Liposomes were sedimented using ultracentrifugation (100,000 × *g*, 1 h, room temperature), and the amount of VSTx1 in the supernatant was confirmed to be minimal using HPLC. Liposome pellets were transferred into glass NMR containers via centrifugation. The sample was lyophilized and rehydrated with H_2O to the final water-to-lipid molar ratio ($R_{W/L}$) of 30:1.

Oriented multilayer samples were prepared by dissolving the VSTx1 peptide in a mixture of trifluoroethanol and hexafluoroisopropanol (1:2 ratio) and the lipid in chloroform (VSTx:lipid ratio of 1 mol%). Treatment of VSTx1 in a mixture of trifluoroethanol and hexafluoroisopropanol did not result in deterioration of peptide structure or inhibitory qualities as detected by CD spectroscopy (Fig. S1) and electrophysiology recordings (Fig. 1*B*). The solution was deposited on a glass slide, dried under vacuum, and rehydrated

to 86% relative humidity. Smoothed order parameter profiles were calculated as described (73).

All spectra were recorded on a 800-MHz Bruker AV800 spectrometer (Bruker Biospin) using either a static ^{1}H/X double-resonance probe with a home-built flat coil for oriented samples, or a triple-resonance ^{1}H/^{13}C/^{2}H 4-mm MAS probe for liposome pellets, operated without spinning, at a ^{2}H NMR resonance frequency of 122.8 MHz. ^{2}H NMR spectra were acquired with a quadrupolar echo pulse sequence (59): 90° pulse flat-coil probe, 4.5 μs, echo delay time, 50 μs; MAS probe, 90° pulse, 5.2 μs, echo delay time, 25 μs; acquisition delay time, both probes, 0.2 s, spectral width, 500 kHz. Powder pattern ^{2}H NMR spectra were de-Paked (74, 75). The order parameter $S(n)$ of the C–D bonds were calculated according to the following formula:

$$S(n) = \Delta\nu_Q(n) / (3/4 * e^2 qQ/h),$$

where n is the carbon atom number of the palmitoyl chain, $\Delta\nu_Q(n)$ is quadrupolar splitting, and e^2qQ/h is the quadrupolar coupling constant (167 kHz for deuterons in a C–D bond). The hydrophobic thickness of the bilayers was calculated from chain order parameters as described by ref. 61. Processing of NMR data and spectral analysis were performed with a program written for Mathcad (PTC).

Neutron Diffraction. Neutron diffraction measurements were performed using the MAGIk (formerly AND/R) Instrument at the National Institute of Standards and Technology Center for Neutron Research (Gaithersburg, MD) (63). Lamellar samples containing 1,000–2,000 bilayers were prepared in a similar fashion as for solid-state NMR experiments using oriented bilayers at partial hydration. Samples were hydrated at 86% relative humidity. Monochromatic cold neutrons of wavelength $\lambda = 5$ Å and a wavelength spread $\Delta\lambda/\lambda = 1\%$ were diffracted by the samples and counted with a pencil-type ^{3}He gas-filled detector. Diffraction from (h, 0, 0) set of planes of the aligned lamellar samples, probing the axis perpendicular to the bilayer plane (z axis), was used to determine the one-dimensional SLD profiles of the bilayer. Typically, five Bragg diffraction peaks (h = 1–5) were observed for each of the measured samples. Sets of five structure factors $F(h = 1 \div 5)$ were obtained as square root of the integrated intensities, corrected for background, absorption, and extinction, and their phases determined by deuterium contrast, as previously described (62, 76, 77). Structure factors were converted, by Fourier synthesis, into a projection of the unit cell content (half bilayer plus associated water) onto the bilayer normal (78), and SLD was calculated according to the following equation:

$$SLD(z) = A_{uc}\sum_i w_i\rho_i + \frac{2}{d}\sum_h f(h)\cos\left(\frac{2\pi\, h\, z}{d}\right).$$

The first term is the average SLD of the compositional unit cell of the bilayer that can be described here as a cylinder with cross-sectional area A_{uc} measured along the surface of the bilayer, and height $d/2$, measured along the z axis. All components of the bilayer (lipid, water, VSTx1) contribute their SLD (ρ_i) and their molar fraction (w_i) to the unit cell. The second term of the equation describes the fluctuations in SLD about the average, where $f(h)$ are the calibrated structure factors. A_{uc} varies dramatically with composition, hydration, or temperature. Therefore, for convenience, all profiles are determined here on an "absolute-relative" scale (79) that leaves A_{uc} undetermined. A set of structure factors is determined for each sample composition or measurement condition. To determine a calibration (scale) factor for each set, we used reference samples containing D4-lipid [POPC with four deuterium atoms in the phosphocholine –(CH_2–CH_2)– groups] for calibration (62). Deuterium is introduced at specific locations in the lipids or VSTx1 to highlight different regions of interest in the lipid bilayer or the protein. Although the molecular structure is not affected by this isotopic exchange, contrast is created due to higher neutron scattering length of deuterium relative to hydrogen. The profile of the deuterium across the bilayer is determined by the Fourier synthesis of the structure factor differences (deuterium difference) between two independently measured samples: a deuterated sample and an equivalent hydrogenated sample.

Determining the Orientation of VXT1 in the Bilayer. To determine the orientation of VSTx1 in bilayers from neutron diffraction data, sets of five statistically significant structure factors, scaled to reflect the composition of the unit cell, were determined for the pair of samples: deuterated versus non-deuterated, as explained above. These sets and their SDs (Table S2, D-VSTx1) were used to calculate the SLD profile of the deuterated patch and its associated profile uncertainties (Fig. 5), and constitute here the experimental data for fitting purposes. For modeling of the deuterium distribution, we used the available NMR solution structure for VSTx1 in which deuterium atoms are replaced for hydrogens at the specified locations. Each deuterium atom was represented by a Gaussian distribution whose width can be described in terms of the thermal B factor, analogous to the Debye–Waller temperature factor, that represents a measure of the amplitude of the thermal fluctuations of an atom around its mean position (z_D) (80). By mass spectroscopy analysis, we found that 96% of an expected total of 34 deuterium atoms is present is the deuterated sample. The 4% deuterium unaccounted for was converted into a scale factor in the model. With this information, we applied rigid body rotations of the toxin around its long axis (θx) and an axis perpendicular to that (θy), and translation along the z axis (Tz), until the envelope of all Gaussian distributions describing the deuterium atoms projected on the z axis best approximated the experimental data. A weighted least-square minimization procedure was applied using the standard Levenberg–Marquardt algorithm (81), starting with various sets of initial fit parameters (θx, θy, and B) in an exhaustive search for the best solution. The procedure was performed for a few different conformers of the NMR solution structure that all converged to the same overall orientation of the toxin, as described in *Results*. In using this procedure, we made three reasonable assumptions. First, we assumed that the structure of the VSTx1 does not change significantly upon membrane partitioning, given the rigidity conferred by the three disulfide bonds and the absence of any detectable changes in the CD spectra of the toxin in the presence of membranes (Fig. S1). Second, all deuterium atoms were assigned the same thermal B factor. Because of the very high thermal disorder of the bilayer, there is no reason to expect significant differences in B factors among the side chains. We determined that the B factor for the lipid (–CH_2–CH_2–) group takes a value of 300–400 Å^2. We expect similar values for the B factor describing the deuterium atoms in VSTx1. Indeed, our fitting procedure yields B factors of ~220 Å^2 for the individual deuterium atoms. For a thorough exploration of the solutions space, allowed by the measured uncertainties in the structure factors, we applied a Monte Carlo sampling procedure (78) by which a few hundred sets of structure factors selected randomly from normal distributions around their measured values were tested. Only singular solutions were found that satisfied the criteria described above (Fig. S4). Each model for the deuterium atoms (*Model*) was compared with the experimental data (*Exp*) (Table S2, D-VSTx1) using a weighted Chi-squared minimization routine as follows:

$$Exp_h = \Delta f = fD - fH$$

$$Model_h = C * \sum_z e^{-Bh^2/(2d)^2}\cos\left(\frac{2\pi h z_D}{d}\right)$$

$$Chisq = \sum_h \frac{(Exp_h - Model_h)^2}{\sigma^2_{exp}}.$$

The constant $C = 2*c_D*(b_D - b_H)$, accounts for the molar fraction of deuterium in the sample (c_D) per composition unit cell, and the difference between the scattering length for deuterium and hydrogen ($b_D - b_H$) = 1.04×10^{-4} Å.

ACKNOWLEDGMENTS. We thank Howard Jaffe, Tomohiro Kimura, David Worcester, Joseph Mindell, and members of the K.J.S. and S.W. laboratories for helpful discussions. We thank Tomohiro Kimura for oriented sample NMR probe-head design. We also thank the NINDS protein sequencing facility for mass spectrometry and peptide sequencing. This work was supported by the Intramural Research Programs of the NINDS–NIH (K.J.S.) and National Institute on Alcohol Abuse and Alcoholism–NIH (K.G.), NIH Grant GM74637 (to S.W.), and Program Project GM86685 from NINDS and National Institute of General Medical Sciences (to S.W.). We are grateful for the National Institute of Standards and Technology, US Department of Commerce, in providing the neutron research facilities used for neutron diffraction experiments.

1. Banerjee A, Lee A, Campbell E, Mackinnon R (2013) Structure of a pore-blocking toxin in complex with a eukaryotic voltage-dependent K^+ channel. *eLife* 2:e00594.
2. Miller C (1995) The charybdotoxin family of K^+ channel-blocking peptides. *Neuron* 15(1):5–10.
3. Swartz KJ (2007) Tarantula toxins interacting with voltage sensors in potassium channels. *Toxicon* 49(2):213–230.
4. Bosmans F, Swartz KJ (2010) Targeting voltage sensors in sodium channels with spider toxins. *Trends Pharmacol Sci* 31(4):175–182.

5. Alabi AA, Bahamonde MI, Jung HJ, Kim JI, Swartz KJ (2007) Portability of paddle motif function and pharmacology in voltage sensors. *Nature* 450(7168):370–375.
6. Craik DJ, Daly NL, Waine C (2001) The cystine knot motif in toxins and implications for drug design. *Toxicon* 39(1):43–60.
7. Schmalhofer WA, et al. (2009) A KV2.1 gating modifier binding assay suitable for high throughput screening. *Channels (Austin)* 3(6):437–447.
8. Kaczorowski GJ, McManus OB, Priest BT, Garcia ML (2008) Ion channels as drug targets: The next GPCRs. *J Gen Physiol* 131(5):399–405.
9. Middleton RE, et al. (2002) Two tarantula peptides inhibit activation of multiple sodium channels. *Biochemistry* 41(50):14734–14747.
10. Swartz KJ, MacKinnon R (1995) An inhibitor of the Kv2.1 potassium channel isolated from the venom of a Chilean tarantula. *Neuron* 15(4):941–949.
11. Lampe RA, et al. (1993) Isolation and pharmacological characterization of omega-grammotoxin SIA, a novel peptide inhibitor of neuronal voltage-sensitive calcium channel responses. *Mol Pharmacol* 44(2):451–460.
12. McDonough SI, Lampe RA, Keith RA, Bean BP (1997) Voltage-dependent inhibition of N- and P-type calcium channels by the peptide toxin omega-grammotoxin-SIA. *Mol Pharmacol* 52(6):1095–1104.
13. Suchyna TM, et al. (2000) Identification of a peptide toxin from *Grammostola spatulata* spider venom that blocks cation-selective stretch-activated channels. *J Gen Physiol* 115(5):583–598.
14. Suchyna TM, et al. (2004) Bilayer-dependent inhibition of mechanosensitive channels by neuroactive peptide enantiomers. *Nature* 430(6996):235–240.
15. Bae C, Sachs F, Gottlieb PA (2011) The mechanosensitive ion channel Piezo1 is inhibited by the peptide GsMTx4. *Biochemistry* 50(29):6295–6300.
16. Baconguis I, Gouaux E (2012) Structural plasticity and dynamic selectivity of acid-sensing ion channel-spider toxin complexes. *Nature* 489(7416):400–405.
17. Dawson RJ, et al. (2012) Structure of the acid-sensing ion channel 1 in complex with the gating modifier Psalmotoxin 1. *Nat Commun* 3:936.
18. Chen X, Kalbacher H, Gründer S (2006) Interaction of acid-sensing ion channel (ASIC) 1 with the tarantula toxin psalmotoxin 1 is state dependent. *J Gen Physiol* 127(3):267–276.
19. Chen X, Kalbacher H, Gründer S (2005) The tarantula toxin psalmotoxin 1 inhibits acid-sensing ion channel (ASIC) 1a by increasing its apparent H^+ affinity. *J Gen Physiol* 126(1):71–79.
20. Salinas M, et al. (2006) The receptor site of the spider toxin PcTx1 on the proton-gated cation channel ASIC1a. *J Physiol* 570(Pt 2):339–354.
21. Escoubas P, Bernard C, Lambeau G, Lazdunski M, Darbon H (2003) Recombinant production and solution structure of PcTx1, the specific peptide inhibitor of ASIC1a proton-gated cation channels. *Protein Sci* 12(7):1332–1343.
22. Bohlen CJ, et al. (2010) A bivalent tarantula toxin activates the capsaicin receptor, TRPV1, by targeting the outer pore domain. *Cell* 141(5):834–845.
23. Bae C, et al. (2012) High yield production and refolding of the double-knot toxin, an activator of TRPV1 channels. *PLoS One* 7(12):e51516.
24. Takahashi H, et al. (2000) Solution structure of hanatoxin1, a gating modifier of voltage-dependent K^+ channels: Common surface features of gating modifier toxins. *J Mol Biol* 297(3):771–780.
25. Takeuchi K, et al. (2002) Solution structure of ω-grammotoxin SIA, a gating modifier of P/Q and N-type Ca^{2+} channel. *J Mol Biol* 321(3):517–526.
26. Lee CW, et al. (2004) Solution structure and functional characterization of SGTx1, a modifier of Kv2.1 channel gating. *Biochemistry* 43(4):890–897.
27. Jung HJ, et al. (2005) Solution structure and lipid membrane partitioning of VSTx1, an inhibitor of the KvAP potassium channel. *Biochemistry* 44(16):6015–6023.
28. Lee S, et al. (2010) Solution structure of GxTX-1E, a high-affinity tarantula toxin interacting with voltage sensors in Kv2.1 potassium channels. *Biochemistry* 49(25):5134–5142.
29. Oswald RE, Suchyna TM, McFeeters R, Gottlieb P, Sachs F (2002) Solution structure of peptide toxins that block mechanosensitive ion channels. *J Biol Chem* 277(37):34443–34450.
30. Pallaghy PK, Nielsen KJ, Craik DJ, Norton RS (1994) A common structural motif incorporating a cystine knot and a triple-stranded beta-sheet in toxic and inhibitory polypeptides. *Protein Sci* 3(10):1833–1839.
31. Bernard C, et al. (2000) Solution structure of hpTX2, a toxin from *Heteropoda venatoria* spider that blocks Kv4.2 potassium channel. *Protein Sci* 9(11):2059–2067.
32. Swartz KJ, MacKinnon R (1997b) Mapping the receptor site for hanatoxin, a gating modifier of voltage-dependent K^+ channels. *Neuron* 18(4):675–682.
33. Li-Smerin Y, Swartz KJ (1998) Gating modifier toxins reveal a conserved structural motif in voltage-gated Ca^{2+} and K^+ channels. *Proc Natl Acad Sci USA* 95(15):8585–8589.
34. Li-Smerin Y, Swartz KJ (2000) Localization and molecular determinants of the Hanatoxin receptors on the voltage-sensing domains of a K^+ channel. *J Gen Physiol* 115(6):673–684.
35. Li-Smerin Y, Swartz KJ (2001) Helical structure of the COOH terminus of S3 and its contribution to the gating modifier toxin receptor in voltage-gated ion channels. *J Gen Physiol* 117(3):205–218.
36. Bosmans F, Martin-Eauclaire MF, Swartz KJ (2008) Deconstructing voltage sensor function and pharmacology in sodium channels. *Nature* 456(7219):202–208.
37. Jiang Y, et al. (2003) X-ray structure of a voltage-dependent K^+ channel. *Nature* 423(6935):33–41.
38. Jiang Y, Ruta V, Chen J, Lee A, MacKinnon R (2003) The principle of gating charge movement in a voltage-dependent K^+ channel. *Nature* 423(6935):42–48.
39. Ruta V, Chen J, MacKinnon R (2005) Calibrated measurement of gating-charge arginine displacement in the KvAP voltage-dependent K^+ channel. *Cell* 123(3):463–475.
40. Swartz KJ (2008) Sensing voltage across lipid membranes. *Nature* 456(7224):891–897.
41. Bezanilla F (2008) How membrane proteins sense voltage. *Nat Rev Mol Cell Biol* 9(4):323–332.
42. Swartz KJ, MacKinnon R (1997a) Hanatoxin modifies the gating of a voltage-dependent K^+ channel through multiple binding sites. *Neuron* 18(4):665–673.
43. Lee HC, Wang JM, Swartz KJ (2003) Interaction between extracellular Hanatoxin and the resting conformation of the voltage-sensor paddle in Kv channels. *Neuron* 40(3):527–536.
44. Phillips LR, et al. (2005) Voltage-sensor activation with a tarantula toxin as cargo. *Nature* 436(7052):857–860.
45. Bosmans F, Puopolo M, Martin-Eauclaire MF, Bean BP, Swartz KJ (2011) Functional properties and toxin pharmacology of a dorsal root ganglion sodium channel viewed through its voltage sensors. *J Gen Physiol* 138(1):59–72.
46. Milescu M, Lee HC, Bae CH, Kim JI, Swartz KJ (2013) Opening the shaker K^+ channel with hanatoxin. *J Gen Physiol* 141(2):203–216.
47. Milescu M, et al. (2007) Tarantula toxins interact with voltage sensors within lipid membranes. *J Gen Physiol* 130(5):497–511.
48. Milescu M, et al. (2009) Interactions between lipids and voltage sensor paddles detected with tarantula toxins. *Nat Struct Mol Biol* 16(10):1080–1085.
49. Lee SY, MacKinnon R (2004) A membrane-access mechanism of ion channel inhibition by voltage sensor toxins from spider venom. *Nature* 430(6996):232–235.
50. Posokhov YO, Gottlieb PA, Morales MJ, Sachs F, Ladokhin AS (2007) Is lipid bilayer binding a common property of inhibitor cysteine knot ion-channel blockers? *Biophys J* 93(4):L20–L22.
51. Krepkiy D, Gawrisch K, Swartz KJ (2012) Structural interactions between lipids, water and S1-S4 voltage-sensing domains. *J Mol Biol* 423(4):632–647.
52. Long SB, Tao X, Campbell EB, MacKinnon R (2007) Atomic structure of a voltage-dependent K^+ channel in a lipid membrane-like environment. *Nature* 450(7168):376–382.
53. Schmidt D, MacKinnon R (2008) Voltage-dependent K^+ channel gating and voltage sensor toxin sensitivity depend on the mechanical state of the lipid membrane. *Proc Natl Acad Sci USA* 105(49):19276–19281.
54. Schmidt D, Jiang QX, MacKinnon R (2006) Phospholipids and the origin of cationic gating charges in voltage sensors. *Nature* 444(7120):775–779.
55. Xu Y, Ramu Y, Lu Z (2008) Removal of phospho-head groups of membrane lipids immobilizes voltage sensors of K^+ channels. *Nature* 451(7180):826–829.
56. Ramu Y, Xu Y, Lu Z (2006) Enzymatic activation of voltage-gated potassium channels. *Nature* 442(7103):696–699.
57. Jung HH, et al. (2010) Structure and orientation of a voltage-sensor toxin in lipid membranes. *Biophys J* 99(2):638–646.
58. Ladokhin AS (2014) Measuring membrane penetration with depth-dependent fluorescence quenching: Distribution analysis is coming of age. *Biochim Biophys Acta* 1838(9):2289–2295.
59. Davis JH, Jeffrey KR, Bloom M, Valic MI, Higgs TP (1976) Quadrupolar echo deuteron magnetic-resonance spectroscopy in ordered hydrocarbon chains. *Chem Phys Lett* 42(2):390–394.
60. Davis JH (1979) Deuterium magnetic resonance study of the gel and liquid crystalline phases of dipalmitoyl phosphatidylcholine. *Biophys J* 27(3):339–358.
61. Nagle JF (1993) Area/lipid of bilayers from NMR. *Biophys J* 64(5):1476–1481.
62. Krepkiy D, et al. (2009) Structure and hydration of membranes embedded with voltage-sensing domains. *Nature* 462(7272):473–479.
63. Dura JA, et al. (2006) AND/R: Advanced neutron diffractometer/reflectometer for investigation of thin films and multilayers for the life sciences. *Rev Sci Instrum* 77(7):74301–7430111.
64. Tardieu A, Luzzati V, Reman FC (1973) Structure and polymorphism of the hydrocarbon chains of lipids: a study of lecithin-water phases. *J Mol Biol* 75(4):711–733.
65. Wee CL, Gavaghan D, Sansom MS (2008) Lipid bilayer deformation and the free energy of interaction of a Kv channel gating-modifier toxin. *Biophys J* 95(8):3816–3826.
66. Winterfield JR, Swartz KJ (2000) A hot spot for the interaction of gating modifier toxins with voltage-dependent ion channels. *J Gen Physiol* 116(5):637–644.
67. Yau WM, Wimley WC, Gawrisch K, White SH (1998) The preference of tryptophan for membrane interfaces. *Biochemistry* 37(42):14713–14718.
68. Wang JM, et al. (2004) Molecular surface of tarantula toxins interacting with voltage sensors in K(v) channels. *J Gen Physiol* 123(4):455–467.
69. Ladokhin AS, Jayasinghe S, White SH (2000) How to measure and analyze tryptophan fluorescence in membranes properly, and why bother? *Anal Biochem* 285(2):235–245.
70. Ladokhin AS (1999) Analysis of protein and peptide penetration into membranes by depth-dependent fluorescence quenching: Theoretical considerations. *Biophys J* 76(2):946–955.
71. Ladokhin AS (1997) Distribution analysis of depth-dependent fluorescence quenching in membranes: A practical guide. *Methods Enzymol* 278:462–473.
72. McIntosh TJ, Holloway PW (1987) Determination of the depth of bromine atoms in bilayers formed from bromolipid probes. *Biochemistry* 26(6):1783–1788.
73. Lafleur M, Fine B, Sternin E, Cullis PR, Bloom M (1989) Smoothed orientational order profile of lipid bilayers by 2H-nuclear magnetic resonance. *Biophys J* 56(5):1037–1041.
74. Sternin E, Bloom M, Mackay AL (1983) De-Pake-ing of NMR spectra. *J Magn Reson* 55(2):274–282.
75. Mccabe MA, Wassall SR (1995) Fast-Fourier-transform dePaking. *J Magn Reson B* 106(1):80–82.
76. Worcester DL, Franks NP (1976) Structural analysis of hydrated egg lecithin and cholesterol bilayers. II. Neutrol diffraction. *J Mol Biol* 100(3):359–378.
77. Zaccai G, Büldt G, Seelig A, Seelig J (1979) Neutron diffraction studies on phosphatidylcholine model membranes. II. Chain conformation and segmental disorder. *J Mol Biol* 134(4):693–706.
78. Wiener MC, King GI, White SH (1991) Structure of a fluid dioleoylphosphatidylcholine bilayer determined by joint refinement of x-ray and neutron diffraction data. I. Scaling of neutron data and the distributions of double bonds and water. *Biophys J* 60(3):568–576.
79. Wiener MC, White SH (1992) Structure of a fluid dioleoylphosphatidylcholine bilayer determined by joint refinement of x-ray and neutron diffraction data. III. Complete structure. *Biophys J* 61(2):434–447.
80. Warren BE (1969) *X-Ray Diffraction* (Addison-Wesley, Reading, MA).
81. Bevington PR (1969) *Data Reduction and Error Analysis for the Physical Sciences* (McGraw-Hill, New York).

Supporting Information

Mihailescu et al. 10.1073/pnas.1415324111

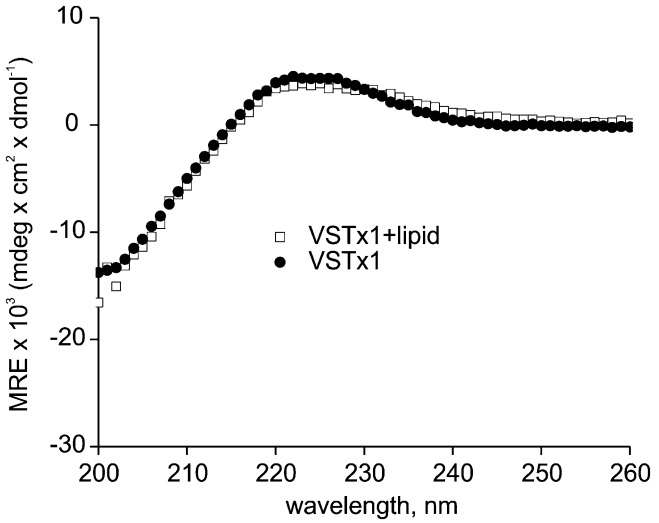

Fig. S1. CD spectra of VSTx1 in the absence and presence of lipids. VSTx1 concentration is 10 μM and POPC:POPG liposomes were added at concentration of 1 mM.

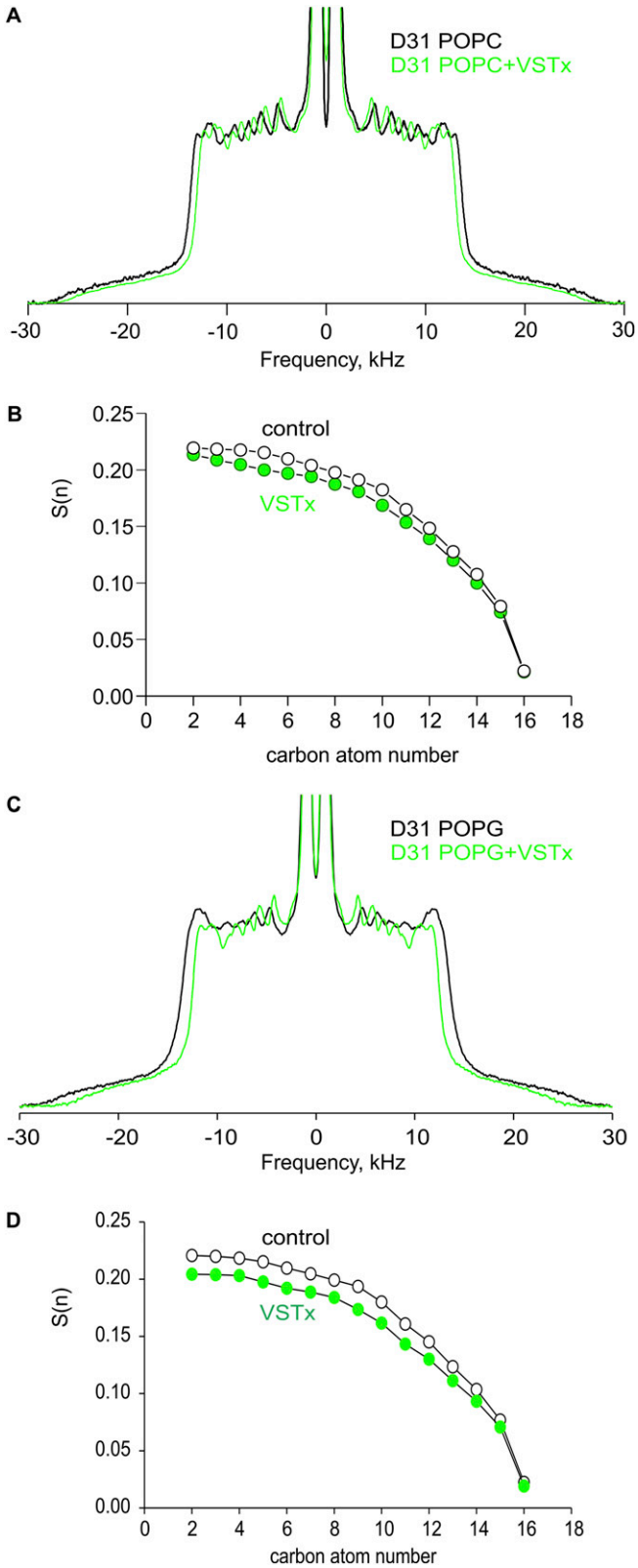

Fig. S2. Changes in the C–D ^{2}H NMR lipid order parameters for liposomes in the absence and presence of VSTx1. (*A*) Powder pattern ^{2}H NMR spectra of D31-POPC:POPG (1:1) mixture. A spectral width of 500 kHz was used for samples studied in the liquid-crystalline phase (295.1 K). (*B*) Order parameters of lipid C–D bonds calculated by the dePakeing procedure. (*C*) Powder pattern ^{2}H NMR spectra of D31-POPG. (*D*) Order parameters of lipid C–D bonds calculated by the dePakeing procedure. In all cases, the ratio of VSTx1 to lipid is 1 mol%.

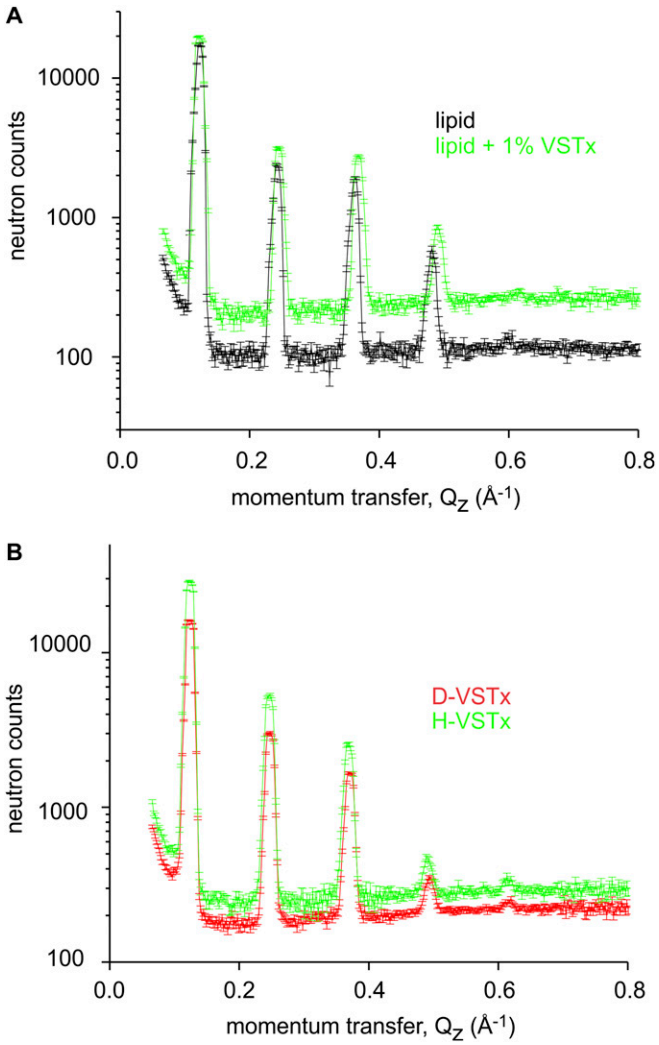

Fig. S3. Neutron diffraction data obtained for lipid multilayers with or without VSTx1. (*A*) Raw diffraction data for POPC:POPG (1:1) alone (black) and the POPC:POPG (1:1) in the presence of 1 mol% VSTx1 (green). Measurements were done at 86% relative humidity at 25 °C. The diffraction signal was collected in a (Θ-2Θ) specular mode, maintaining the momentum transfer normal to the bilayer planes. Water contrast ($H_2O/^2H_2O$) measurements were used to obtain the phase information for the lipid bilayer structure factors. The repeat distances (*d*) of the lamellar structures were 52.5 Å for lipid and 51.6 Å for lipid plus 1% toxin. (*B*) Neutron diffraction data from POPC/POPG lipid multilayers containing 1.75% VSTx1 in either protonated (green) or patch-deuterated forms (red). Data are presented as measured, before corrections and scaling. Repeat spacing is 51.2 Å.

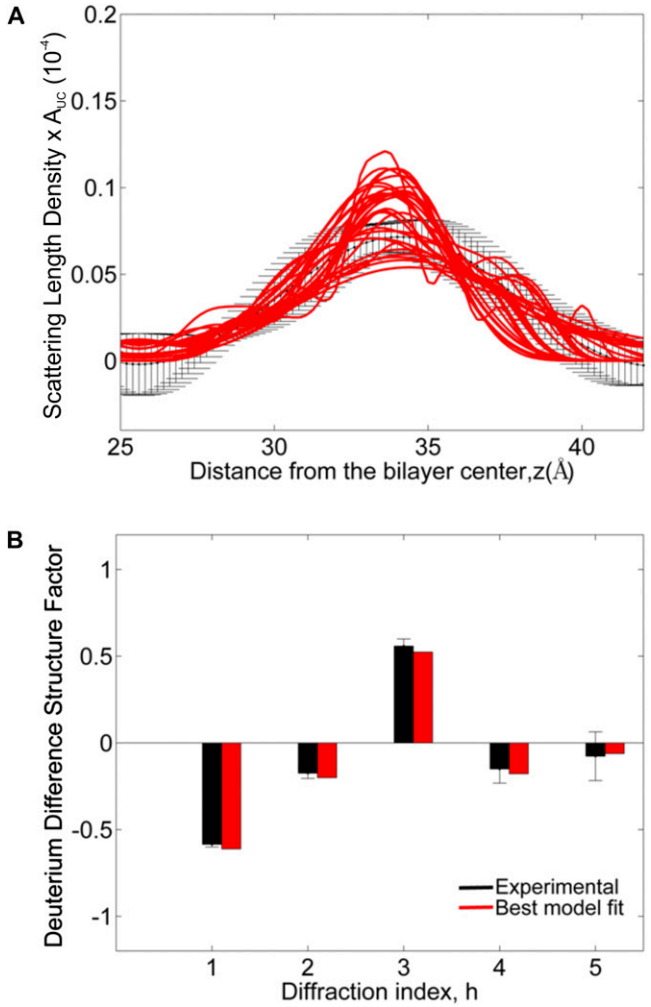

Fig. S4. Illustration of a Monte Carlo procedure where model fitting was performed using mock sets of structure factors with values randomly selected from normal distributions around their measured value (Δf). (*A*) SLD profiles of the deuterium patch resulting from trial structure factor datasets (black) and fitting attempts (red). Typically, from hundreds of attempts, only singular solutions were found that were considered reasonable, under the criteria described in *Experimental Procedures*. Those solutions for the toxin orientation agree with the best fit results found overall, as described in *Results*. (*B*) Measured difference structure factors for the deuterated patch (black) and best-fit solution (red).

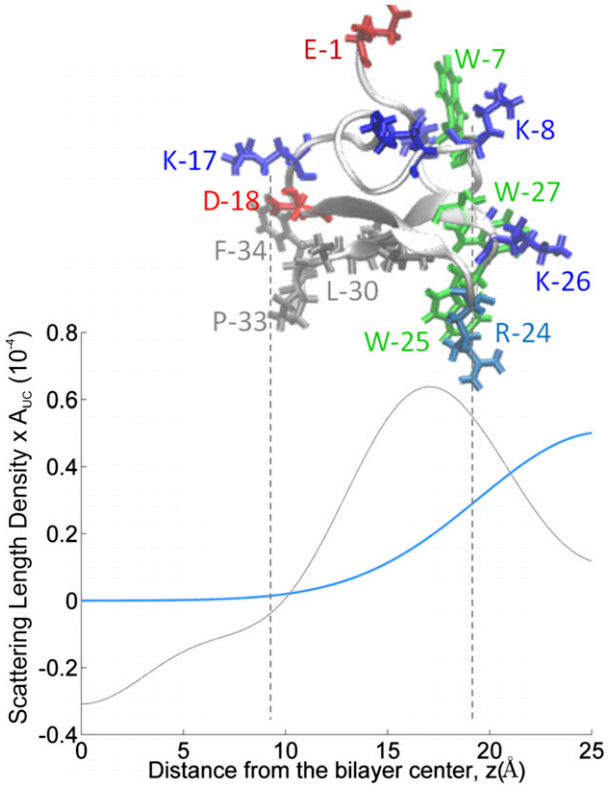

Fig. S5. VSTx1 position and orientation from model fitting. Modeling results indicate that the C terminus together with the (K-17, D-18) pair are positioned in the bilayer below the phosphate headgroups, facing the hydrocarbon core. A layer of basic amino acids (blue) point toward the water phase. The three tryptophan residues form a ridge aligning with the lipid headgroup–water interface. Representative α-carbon *z* positions of residues in the preferred orientation (results are from model fitting using NMR solution structure conformer number 7 as a starting conformation): *z*(E-1) = 13.3 Å; *z*(K-8) = 22.3 Å; *z*(R-24) = 22.0 Å; *z*(L-30) = 13.9 Å; *z*(K-17) = 8.5 Å; *z*(D-18) = 8.9 Å; *z*(F-34) = 8.8 Å. Also shown are the SLD profiles of the lipid bilayer (gray) and water distribution (blue).

Table S1. Structure factors for diffraction from lipid multilayers of POPC/POPG (1/1 molar ratio), and POPC/POPG containing 1 mol% VSTx1

Diffraction index	*fH* (lipid)	Δ*f* (lipid) D31	*fH* (1% VSTx1)	Δ*f* (1% VSTx1) D31
1	−5.744 ± 0.006	14.011 ± 0.018	−8.952 ± 0.016	14.576 ± 0.034
2	−4.932 ± 0.008	−4.482 ± 0.027	−4.753 ± 0.026	−3.286 ± 0.042
3	4.851 ± 0.011	−1.788 ± 0.042	4.382 ± 0.043	−1.307 ± 0.084
4	−2.524 ± 0.023	1.157 ± 0.073	−2.012 ± 0.078	0.420 ± 0.174
5	−1.135 ± 0.055	0.347 ± 0.140	−0.553 ± 0.178	−0.408 ± 0.219

POPG deuterated in the palmitoyl chain (D31) was used to determine the chain distribution by deuterium difference analysis. The amplitudes of the measured structure factors were rescaled using the D31 distribution as a calibration reference, and knowing to best approximation the sample composition. Uncertainties in the structure factors represent 1 SD due to counting statistics.

Table S2. Calibrated structure factors used to construct the SLD profiles shown in Fig. 4

Diffraction index	*fH* H_2O	Δ*f* (^2H_2O)	Δ*f* –$(CD2)_2$–	Δ*f* D-VSTx1	Δ*f*_model D-VSTx1
1	−8.714 ± 0.010	−5.976 ± 0.015	−3.013 ± 0.013	−0.585 ± 0.015	−0.612
2	−5.058 ± 0.023	3.068 ± 0.036	0.739 ± 0.029	−0.175 ± 0.030	−0.201
3	4.229 ± 0.034	−0.764 ± 0.045	0.961 ± 0.040	0.559 ± 0.041	0.524
4	−1.461 ± 0.066	−0.038 ± 0.100	−1.305 ± 0.090	−0.151 ± 0.081	−0.178
5	−0.910 ± 0.096	0.042 ± 0.189	0.806 ± 0.169	−0.077 ± 0.141	−0.062

Deuterium difference structure factors (Δ*f*) for diffraction from lipid multilayers containing deuterated species: water (^2H_2O), D4–phosphocholine, and deuterated toxin (D-VSTx1) relative to the hydrogenated homologue (*fH*). The deuterium peak corresponding due to D4 label was used for calibration. Uncertainties in the structure factors represent 1 SD derived from counting statistics in the measured neutron counts. Structure factors for a model that best describe the experimental D-VSTx1 distribution (Fig. S4*B*) are shown in the last column.

Table S3. Calibrated structure factors (*f*) for diffraction from lipid multilayers containing deuterated VSTx1 and increasing amounts of ^2H_2O in the hydrating vapor

Diffraction index	*fH* H_2O	*fD* 20% ^2H_2O	*fD* 50% ^2H_2O	*fD* 100% ^2H_2O
1	−9.052 ± 0.010	−15.114 ± 0.011	−23.984 ± 0.016	−39.416 ± 0.022
2	−5.330 ± 0.019	−2.248 ± 0.030	1.683 ± 0.035	8.707 ± 0.026
3	4.802 ± 0.023	4.044 ± 0.033	2.917 ± 0.061	0.825 ± 0.180
4	−1.794 ± 0.048	−1.723 ± 0.043	−1.437 ± 0.108	−1.140 ± 0.111
5	−1.032 ± 0.103	−0.936 ± 0.101	−1.022 ± 0.196	−1.057 ± 0.219